

## Article

# Reflectivity of Cholesteric Liquid Crystals with an Anisotropic Defect Layer Inside

Dariusz Grzelczyk \*  and Jan Awrejcewicz 

Department of Automation, Biomechanics and Mechatronics, Lodz University of Technology,  
90-924 Lodz, Poland; jan.awrejcewicz@p.lodz.pl

\* Correspondence: [dariusz.grzelczyk@p.lodz.pl](mailto:dariusz.grzelczyk@p.lodz.pl)

Received: 15 June 2020; Accepted: 7 August 2020; Published: 10 August 2020



**Abstract:** In this study, first, we numerically investigated the reflectivity of a cholesteric liquid crystal with an anisotropic defect layer inside. To model optical phenomena in the examined system, a  $4 \times 4$  matrix method was employed. The tests were carried out for different thicknesses of the whole system, different thicknesses of the defect layer, as well as different defect layer locations inside the cell. Next, a cholesteric liquid crystal comprising a defect layer and held between two parallel electrical conductors was also considered. In this case, the optical properties of the system could also be adjusted by an external applied electric field. Some interesting simulation results of the reflection coefficient (i.e., the fraction of electromagnetic energy reflected) were obtained, illustrated, and discussed. The simulation results showed a significant influence of both the defect and the external electric field on the selective reflection phenomenon, and the possibility of controlling the shape of the reflection spectrum. Finally, some potential applications of the analyzed optical system were discussed.

**Keywords:** photonic materials; cholesteric liquid crystal; optical metrology; reflectivity; reflection; bandgap; defect mode; defect layer; director field; electric field

## 1. Introduction

Photonic crystals consisting of artificial or organic self-organizing periodic structures have opened up new possible applications in modern electronic devices. Some of the possible practical applications of such materials in different branches of science and technology can be found, for instance, in recent review papers [1–5]. Especially attractive is the use of cholesteric liquid crystals (CLCs) since the macroscopic properties of such optical structures can be manipulated by external stimuli.

CLCs are organic materials with unique and useful optical properties. They are composed of optically anisotropic and uniaxial elements (molecules), with one major and two minor principal axes, which are also mutually perpendicular locally. In cholesteric liquid crystals, there is a long-range orientational order of the elongated molecules with locally preferred common direction called the director. Whereas in nematic liquid crystals, the elastic forces and torques tend to establish a uniform orientation of the director, the chiral molecules in CLCs lead in equilibrium to a helical arrangement with the director perpendicular to the helix axis [6]. This way, they have a one-dimensional periodic modulation of dielectric constants, which leads to interesting optical effects.

Owing to the optical anisotropy and helical twist, CLCs are characterized by the so-called selective reflection. It means that for the light incident along the helical axis (normal incidence), the circularly polarized light with the same handedness as that of CLC, is totally reflected in the specific wavelength range. The edges of this bandwidth are defined by two sharp optical modes which correspond to circularly polarized standing waves in which the electric field in the bulk of the sample is aligned along either the ordinary or the extraordinary molecular axes [7]. This unique feature of the selective

reflection is widely used in numerous applications such as reflective displays, tunable color filters, or mirrorless lasers [8].

In isotropic periodic media, defects have been created by the removal or addition of a material, or by an alteration of the refractive index of one or a number of elements of photonic crystals [9]. In the anisotropic optical structures considered in this study, defects can be introduced by replacing a part of the host medium with a material that has a different dielectric constant and can make defect modes in the forbidden bands [10]. The defect makes such structures more useful (such as doped semiconductors) and can be successfully used for constructing narrowband filters [11–13], low threshold lasers [14,15], and other optical devices. A broad overview of the properties of all currently existing defective modes in CLCs, including both the proposed theoretical approaches and the performed experimental observations, can be found in monography [16]. In particular, efficient applications of localized modes for low-threshold lasing at the frequencies of localized modes are presented in this study as the most recent achievements in this area.

Generally, two ways to introduce a defect in CLCs have been proposed (and discussed in more detail below): either by replacing a thin layer of the CLC with an isotropic material [10], or by introducing a phase jump in the cholesteric helix [7]. In the first case, in analogy with isotropic periodic structures, a defect can be produced in a helical structure by adding an isotropic layer in the middle of a CLC. In the second case, a chiral twist defect can be created by rotating one part of the sample about its helical axis without separating the two parts.

Yang et al. [10] theoretically studied the reflection and transmission of light from a one-dimensional system consisting of two layers of cholesteric liquid crystal sandwiching a thin layer of the isotropic medium as a defect. Reflection spectra for normal incidence, calculated by using the so-called “faster Berreman method”, were studied to obtain the wavelengths and intensities of defect modes when the refractive index and the thickness of the defect layer were varied.

Gevorgyan and Harutyunyan [17] considered some properties of defect modes in chiral photonic crystals with an anisotropic defect layer. They solved the problem by the Ambartsumian’s layer addition method previously developed for the solution of astrophysical problems of multiple scattering in turbid media, and further extended to optical wave propagation through inhomogeneous media [18]. As a result, the influence of the defect layer thickness variation and its location in the chiral photonic crystal on defect mode properties were investigated. However, the amplitudes of the reflected and transmitted fields related to the incident wave were expressed by using  $2 \times 2$  Jones matrix method, in which both the effect of refraction and multiple reflections between plate interfaces (dielectric discontinuities) are neglected [19].

Kopp and Genack [7] considered photonic properties of a defect created by twisting one part of an anisotropic structure relative to the rest of the sample. The authors restricted their discussion to samples with a chiral twist of  $90^\circ$  in the center of the sample, which creates a photonic defect at a frequency in the center of the stopband. However, varying the chiral twist angle in the range  $0$ – $180^\circ$  tunes the defect frequency from the low to the high-frequency band edge. The study demonstrated that twisting one part of a chiral photonic structure about its helical axis creates a single circularly polarized localized mode that gives rise to an anomalous crossover in propagation. This is in contrast to a defect in a binary layered medium that produces two orthogonally polarized degenerate localized modes.

In another study, Schmidtke et al. [13] used two layers of a highly cross-linked CLC polymer film to create a phase jump of  $90^\circ$  in the cholesteric structure. They observed experimentally enhanced fluorescence inside the photonic stopband and laser emission due to a photonic defect mode in a dye-doped cholesteric polymer network. The observed emission peak can be attributed to the localized defect mode generated by the phase jump of the cholesteric helix and it agrees with the simulation results of Kopp and Genack [7], who have theoretically predicted the presence of a defect mode in the center of the stopband.

In the study [20], the twist defect mode induced by a discontinuity of the director rotation around the helix axis at an interface of two photopolymerized cholesteric liquid crystal layers has

been experimentally demonstrated in the transmission spectrum. The existing self-organized helical structure of such composite film acts as a one-dimensional photonic crystal. Finally, the authors observed optically pumped laser action based on the twist defect mode.

Ha et al. [21] considered quasi-periodic Fibonacci phase defects in single-pitched cholesteric liquid crystalline systems. Fundamental optical properties were discussed as functions of phase jump (orientational defect angles), unit lengths, and the orders of Fibonacci systems. The performed simulations of reflection spectra demonstrated simultaneous red, green, and blue reflections or multiple photonic bandgaps, and the color of reflections could be controlled by an orientational defect angle.

Motivated by the literature review presented above, in this study, we considered a defect in the form of an anisotropic layer with different thicknesses, different locations of the defect layer inside the analyzed CLC cell, as well as different total thicknesses of the investigated system. To model optical phenomena, we implemented the  $4 \times 4$  matrix method which gives accurate numerical results and was used in many previous papers [9,20–31]. On the contrary to numerous former studies examining the defect modes in nondeformed CLCs, we also investigated the influence of an external electric field applied to the considered CLC optical system with a defect layer inside. This is important from a technological point of view since the investigated optical system can also be additionally tuned during operation by altering the director field of the CLC.

The study is organized as follows. Section 2 presents the considered optical system, i.e., CLC cell with a defect layer inside, sandwiched between two homogenous and isotropic conducting glass samples. Section 3 shortly summarizes the most essential steps in the computational method of the director field of the CLC deformed by an externally applied electric field and the  $4 \times 4$  matrix calculation method. Some interesting numerical simulations of the reflectance obtained for different configurations of the system, different values of the parameters, as well as different director fields of the CLC are reported and discussed in Section 4. Lastly, a brief summary and the conclusions of the study are outlined in Section 5.

## 2. Model of the Considered Optical System

Generally, in a liquid crystal cell under a given boundary condition and an externally applied field, the liquid crystal is in the director field configuration that minimizes the total free energy of this system [32]. In other words, there is a critical amplitude of the electric field below which the internal elastic strength of the liquid crystal exceeds the electric forces; therefore, the system remains undeformed from its base state. When a relatively large external electric field is applied to the cell, the liquid crystal will reorient because of the dielectric interaction between the crystal and the applied field. This bifurcation field-induced reorientation of the liquid crystal is referred to as the Fréedericksz transition [32].

Generally, determining the director field in a cholesteric liquid crystal device is complicated due to the large number of material parameters that characterize it. The tendency of the director to take on a particular spatial distribution can be understood in terms of the well-known elastic continuum theory. For instance, in papers [33–35], the problem of the continuum theory for nematic and cholesteric liquid crystals is exhaustively reported, and, therefore, it is not considered in detail in this study. According to this theory, elastic forces arising from the molecular structure of the material resist any distortion to the director field from its equilibrium state. Such distortions can arise for a number of reasons, including interaction with external electric/magnetic fields, coupling with the material flow of the liquid, or from interactions with confining surfaces [36]. When subjected to competing influences, the director will adjust throughout the sample and, as a result, must be treated as both space- and time-dependent function.

In our analysis, we considered situations, where the electric field interacts with the liquid crystal deformation. In the case of positive dielectric anisotropy of the CLCs, the molecules tend to align parallel to the electric field if voltage (electric field) is applied across the cell. As boundary conditions, we assumed the strong anchoring of the molecules of the CLC at surfaces of substrates and the

deformation of the CLC characterized by the so-called tilt angle and twist angle of the molecules, which depends on the applied electric field, the anisotropy of the electrical permittivity of the liquid crystal, and the anisotropy of the elastic stiffness of the liquid crystal. The anisotropic defect layer is manifested by a locally constant director in the area of the defect layer.

Motivated by the structure of the simplest electro-optic devices, also in our system, a thin layer of a cholesteric liquid crystal is sandwiched between two plates (substrates) which are treated in a way which leads to the surface interaction imposing a specified orientation on the liquid crystal (boundary conditions of the director field). The optical properties of the investigated system can be additionally adjusted by applying an external electric field whose distorting influence on the CLC opposes that of the surfaces.

Figure 1 presents two configurations of the structure of the modeled optical system, i.e., CLC cell with a defect layer (DL) inside, and sandwiched between two (lower and upper substrates) homogenous isotropic media. Figure 1a presents the nondeformed director field, whereas Figure 1b shows the deformed director field caused by the applied electric field. The studied system is located in the right-handed Cartesian coordinate system, where the  $z$ -axis was chosen to be the twist axis of the CLC.

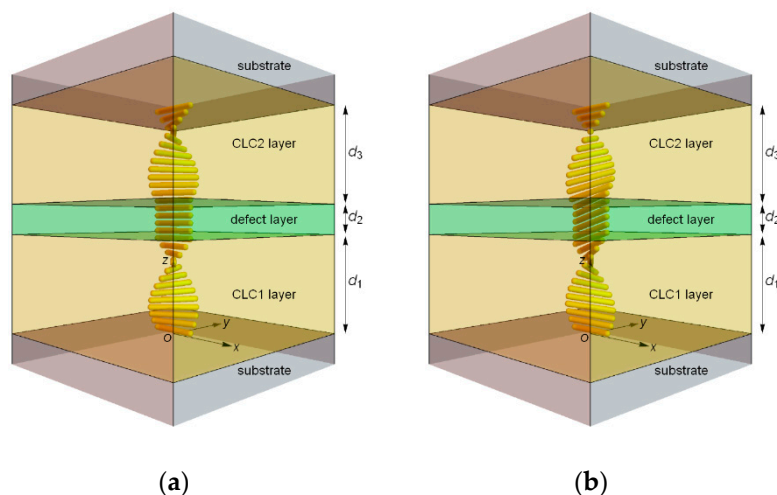


**Figure 1.** A structure of the modeled cholesteric liquid crystal with a defect layer inside that is sandwiched between isotropic substrates, with the orientation of the director: (a) before the electric field is applied; (b) after the electric field is applied. The anisotropic defect layer is manifested by a locally constant director field in the range of the coordinate  $z$  from  $z = d_1$  to  $z = d_1 + d_2$ .

The considered system can be treated as a multilayer system CLC1-DL-CLC2 with thicknesses of  $d_1$ ,  $d_2$ , and  $d_3$ , respectively. In all considered cases, the whole CLC cell with the total thickness  $D = d_1 + d_2 + d_3$  was divided into  $N$  equal multiple elementary layers (sliced into a large number of slabs) of the thickness 1 nm, which was parallel to the substrates (i.e.,  $xy$  plane). Each imaginary elementary  $n$ -th layer can be treated as a homogenous layer with the same orientation of the optical axis, characterized by two angles, i.e., tilt angle and twist angle. The tilt angle was measured from the  $z$ -axis to the direction of the optical axis of the molecule, while the twist angle was measured from the  $x$ -axis to the projection of the optical axis of the molecule on the  $xy$  plane. As a result, each elementary layer can be treated locally as an anisotropic homogenous medium. The spatial period of the helical structure of the CLC characterized by the pitch  $p$  can be easily varied by adding dopants and changing temperature. The ordinary and extraordinary refractive indices were  $n_o = 1.4639$  and  $n_e = 1.5133$ , respectively, whereas the pitch of the right-handed periodic helical structure was  $p = 420$  nm. These values corresponded to the CLC cholesteryl-nonanoate–cholesteryl-chloride–cholesterylacetate (20:15:6) composition at the temperature 298 K [37]. As a result, the light with right circular polarization and normally incident onto a single CLC layer had a bandwidth in the range of  $\lambda \sim (615\text{--}635)$  nm,

whereas the light with the left circular polarization did not have any. The considered system was surrounded by the optical media with the refraction index  $n_s$  on its both sides, equal to  $n_s = 1.4$  (the value that corresponds to glass medium). We assumed that both CLC and DL were not absorbing, and the values of the parameters  $n_s$ ,  $n_o$ , and  $n_e$  did not depend on the wavelength of the incident light.

The incident light propagated in the lower substrate ( $n = 0$ ), then in the CLC1, DL, and CLC2 ( $n = 1, 2, \dots, N$ ), and finally in the upper substrate ( $n = N + 1$ ). The optical axis of the molecules of cholesteric liquid crystals laid on the  $xy$  plane which was parallel to the substrates and changed periodically along the  $z$ -direction. The orientation of the wave vector of the oblique incident nonpolarized beam of monochromatic light with wavelength  $\lambda$  in the lower substrate was represented by angles  $\theta$  and  $\phi$ . The angle  $\theta$  was measured from the  $z$ -axis to the direction of the wave vector of the incident beam of light, while the angle  $\phi$  was measured from the  $x$ -axis to the projection of the director of the wave vector of the incident beam of light on the  $xy$  plane [38,39].

### 3. Calculation Methods

We considered a cholesteric liquid crystal confined between parallel plates at  $z = 0$  and  $z = D$  and subject to strong planar anchoring at these surfaces as boundary conditions. We applied electric potential between the plates giving rise to an electric field parallel to the  $z$ -axis. We took into account the liquid crystal with positive electric anisotropy; therefore, the director tended to align parallel to the local electric field, and at the same time, the director was in competition with the direction of the strong planar anchoring. The deformation of the director occurred in two planes, in which it was possible to describe the director by two angles, namely the abovementioned tilt angle  $\theta_c$  (measured from the  $z$ -axis to the direction of the optical axis of the molecule), and the twist angle  $\phi_c$  (measured from the  $x$ -axis to the projection of the optical axis of the molecule on the  $xy$  plane).

For our calculations, the equations governing the static behavior of the liquid crystal with the variables  $\theta_c$  and  $\phi_c$  of the director field could be obtained from the equations expressing conservation of momentum, angular momentum, and Maxwell equations for the electric displacement field, with the appropriate boundary conditions that reflected the assumption of strong planar anchoring and that the voltage dropped across the considered cell was equal to the applied voltage. The solution of these equations in the nondimensional form depended on nondimensional parameters, i.e., the nondimensional elastic anisotropy, the nondimensional electric anisotropy, and the nondimensional applied voltage. In turn, the abovementioned nondimensional parameters depended on a large number of material parameters that characterized the investigated system. However, from the point of view of the optical properties of the system, such as reflectivity or transmissivity, the spatial distribution of the director had fundamental importance. Therefore, in our research, during the analysis of the considered optical cell in an external electric field, we took into account directly different distributions of the director field that corresponded to different amplitudes  $E$  of the applied electric field. In this way, the obtained results were more general and they could be directly adopted to systems with different material properties, both mechanical and optical.

To model optical phenomena in the analyzed system, we used the  $4 \times 4$  matrix method implemented based on the mathematical formalism presented in [40]. More detailed information regarding the realized computer algorithm of the applied computation technique was presented in detail in one of our previous papers [39]. Below, only the main stages of this method are listed:

- Entering values of all required parameters of the considered optical system, i.e.,  $n_s$ ,  $n_o$ ,  $n_e$ ,  $d_1$ ,  $d_2$ ,  $d_3$ ,  $p$ ,  $\lambda$ ,  $\theta$ , and  $\phi$ ;
- Calculation of the dielectric tensors  $\epsilon(n)$  of the substrates ( $n = 0$  and  $n = N + 1$ ) and the dielectric tensors  $\epsilon(n)$  of the individual elementary crystal/defect layers ( $n = 1, 2, \dots, N$ );
- Calculation of the wave vectors  $\mathbf{k}_\sigma(n)$  of all four elementary waves ( $\sigma = 1, 2, 3, 4$ ) in all elementary layers based on the wave equation;



- Computation of the optical polarization vectors  $\mathbf{p}_o(n)$  of the individual elementary waves representing the directions of the electric field as well as the corresponding vectors  $\mathbf{q}_o(n)$  of the magnetic field;
- Computation of the  $4 \times 4$  transition matrix, which describes the relationships between amplitudes  $A_s, A_p$  of the electric field of the incident waves, amplitudes  $B_s, B_p$  of the electric field of the reflected waves, and amplitudes  $C_s, C_p$  of the electric field of the transmitted waves, both for  $s$  and  $p$  waves, respectively;
- Calculation of the reflection coefficient  $R$  (the fraction of the electromagnetic energy reflected) or optionally the transmission coefficient  $T$  (the fraction of the electromagnetic energy transmitted) of the incident light.

This mathematical approach is an effective technique in describing the optical properties of multi-layered structures and has been widely employed by many researchers in numerous problems, including the investigation of liquid crystal displays [41], the propagation of electromagnetic waves in stratified bianisotropic chiral structures [42], the study of various uniaxial, biaxial dielectric, magnetic materials [43,44], the investigation of the effect of stress-induced anisotropy on localized mode in photonic crystal [31], and the study of different kinds of cells of CLC lasers [45].

#### 4. Results and Discussion

First, we examined the optical system for  $d_1 = d_3 = 10p$  (further referred to as *model 1*) and for different values of the thickness  $d_2$ . In this case, the defect layer was located in the center of the studied cell. A beam of a monochromatic nonpolarized light was incident normally on the surface of the investigated optical system, i.e., perpendicular to the  $xy$  plane. For the sake of completeness and to increase the transparency of the obtained results, the results were presented in a few charts together with the curve obtained for the ideal system as a reference, i.e., without the defect layer (plotted by the dashed curve). The presented simulation results show that the thickness of the defect layer had a significant impact on the shape of the simulated spectral curves, especially in the band of the selective reflection. As one can see, visible dips in the spectral curves were induced by the introduction of the defect layer. Moreover, if the defect layer thickness was changed, the defect mode bandwidth of the incident light was changed too. Generally, the defect effect was present near the center and these curves had a certain asymmetry. However, for some values of the defect layer thickness, this effect was exactly in the center of the bandwidth and the spectral curves were symmetric. It should be noted that a similar effect can also be obtained in another way. For instance, a peak in transmission was observed in the middle of the bandgap, when a system with a spacerless defect was created in sculptured thin films by rotation of the substrate by an additional  $90^\circ$  in the middle of the film fabrication process [12].

The regularities in spectra presented in Figure 2 are easy to understand. When the thickness of the defect increased, the characteristic peak of the maximum value shifted toward the long-wave boundary of the bandwidth, while the second maximum appeared simultaneously on the left side of the spectral curve. For the layer thickness equal to  $0.25p$  (Figure 2a), the spectral curve had a form of two symmetrical maxima with a slightly smaller amplitude around the wavelength of the maximum reflection for the system without the defect. With a further increase in the thickness of the defect (see Figure 2b), a similar situation occurred, but on the other side of the band gap (i.e., mirror image in comparison to the results presented in Figure 2a). For  $d_2 = 0.5p$ , the obtained spectral curve was almost identical to the curve obtained for the system without the defect (only a very small narrowing of the selective reflection bandwidth was visible). Increasing the defect thickness from  $0.5p$  to  $p$  (see Figure 2c,d) caused a similar effect to changing the value of the  $d_2$  parameter in the range from 0 to  $0.5p$  (compare these curves with the curves presented in Figure 2a,b, respectively).

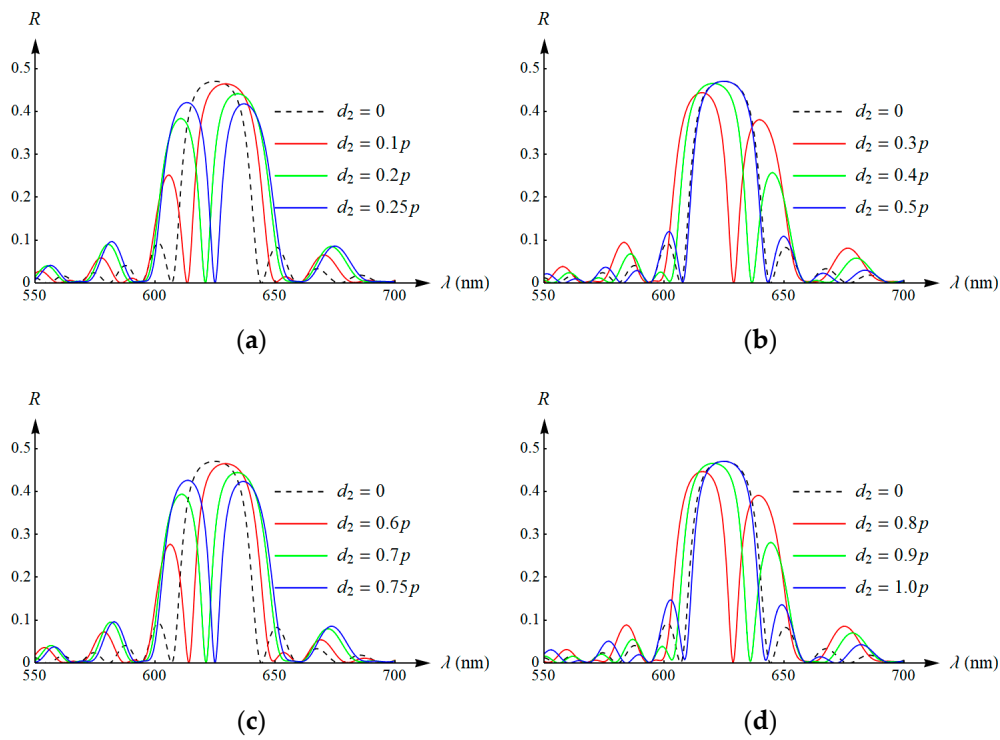


**Figure 2.** Reflection spectra for different values of the thickness  $d_2$  of the defect layer (*model 1*): (a)  $d_2$  equal to  $0.1 p$ ,  $0.2 p$  and  $0.25 p$ ; (b)  $d_2$  equal to  $0.3 p$ ,  $0.4 p$  and  $0.5 p$ ; (c)  $d_2$  equal to  $0.6 p$ ,  $0.7 p$  and  $0.75 p$ ; (d)  $d_2$  equal to  $0.8 p$ ,  $0.9 p$  and  $1.0 p$ .

Figure 3a shows a comparison of curves obtained for the defect layer thickness of  $0.5 p$ ,  $p$ ,  $1.5 p$ , and  $2 p$ , while Figure 3b shows the comparison for  $d_2 = 0.25 p$ ,  $0.75 p$ ,  $1.25 p$ , and  $1.75 p$ , respectively. In the first case (Figure 3a), we obtained similar results to for the system without the defect layer. The increase in the thickness of the defect layer (i.e.,  $d_2$  equal to  $0.5 p$ ,  $p$ ,  $1.5 p$ , or  $2 p$ ) caused only a very small and gradual narrowing of the bandwidth and a significant increase in the amplitude of the side peaks. In turn, for the value of the parameter  $d_2$  tested in Figure 3b (i.e.,  $d_2$  equal to  $0.25 p$ ,  $0.75 p$ ,  $1.25 p$ , and  $1.75 p$ ), two symmetrical peaks were obtained with a slightly smaller amplitude and with a zero reflection coefficient for  $\lambda = (n_0 + n_e) \cdot p/2 \approx 625$  nm. This gradual increase in the defect thickness resulted in a gradual but slight flattening of these spectral curves.

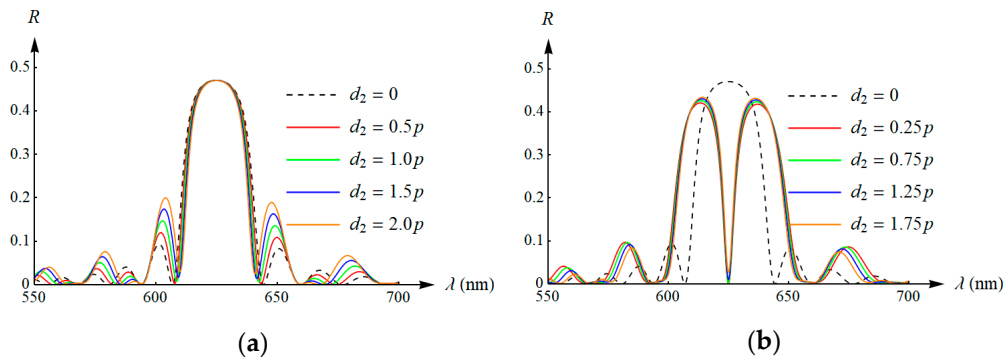


**Figure 3.** Reflection spectra for different values of the thickness  $d_2$  of the defect layer (*model 1*): (a)  $d_2$  equal to  $0.5 p$ ,  $1.0 p$ ,  $1.5 p$  and  $2.0 p$ ; (b)  $d_2$  equal to  $0.25 p$ ,  $0.75 p$ ,  $1.25 p$  and  $1.75 p$ .

Figures 4 and 5 show curves similar to those seen in Figures 2 and 3, but for the optical system with  $d_1 = d_3 = 20 p$  and different values of the thickness  $d_2$  (further referred to as *model 2*). Through

the analysis of the results of numerical simulations for the considered *model 2*, one can come to the same conclusions as for *model 1*. However, for greater values of the total thickness of the considered system, the observed selective reflection phenomenon was more pronounced. In the case of *model 1*, we observed a significant expansion of the selective reflection bandwidth (two adjacent peaks), with the simultaneous reduction in the average amplitude of the reflection coefficient. On the other hand, for *model 2*, the bandwidth extension was slightly smaller, but there was no significant reduction in the reflection coefficient in the bandwidth. This effect resulted from a larger value of the total twist angle of the liquid crystal optical axis, due to which the interference effects inside the crystal was stronger, and the selective reflection coefficient was greater.

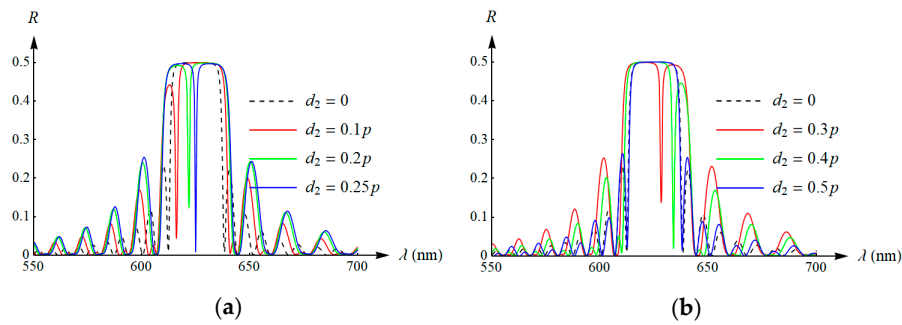


**Figure 4.** Reflection spectra for different values of the thickness  $d_2$  of the defect layer (*model 2*): (a)  $d_2$  equal to  $0.1 p$ ,  $0.2 p$  and  $0.25 p$ ; (b)  $d_2$  equal to  $0.3 p$ ,  $0.4 p$  and  $0.5 p$ .

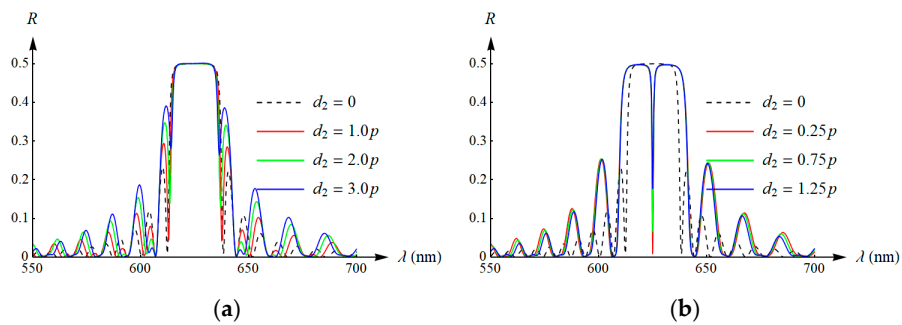


**Figure 5.** Reflection spectra for different values of the thickness  $d_2$  of the defect layer (*model 2*): (a)  $d_2$  equal to  $1.0 p$ ,  $2.0 p$  and  $3.0 p$ ; (b)  $d_2$  equal to  $0.25 p$ ,  $0.75 p$  and  $1.25 p$ .

It is known that in the case of CLCs without defects, the value of the reflection coefficient is almost the same within the entire forbidden band  $\lambda$  in the range  $(n_o p, n_e p)$ . Figure 6 shows the relationship between the reflection coefficient for the wavelength  $\lambda = (n_o + n_e) \cdot p / 2 \approx 625$  nm and the thickness of the defect layer, for both *model 1* and *model 2*. In addition, we also presented similar curves obtained for other wavelengths, i.e.,  $\lambda = n_o \cdot p \approx 615$  nm and  $\lambda = n_e \cdot p \approx 635$  nm.

The simulation results presented in Figure 6 show that the reflection coefficient for individual wavelengths varied significantly depending on the thickness of the defect layer (in the range from 0 to  $0.5 p$ ), which was already observed in previous figures. Figure 6a shows that for the wavelength of 625 nm, the total reflection occurred for  $d_2 = 0$ ,  $0.5 p$  and  $p$ , while no reflection occurred for  $d_2 = 0.25 p$  and  $0.75 p$ . Similar changes occurred for other wavelengths, i.e., 615 and 635 nm, with their maximum and minimum values occurring for other thicknesses of the defect layer. More interesting results are presented in Figure 6b. They were obtained for a greater total thickness of the investigated optical system. In addition, in this case, for the wavelength 625 nm and  $d_2 = 0.25 p$ , there was practically complete quenching of the selective reflection. However, for  $d_2 = 0.75 p$ , the value of the reflection coefficient no longer reached zero. This effect, also for larger values of the  $d_2$  parameter (i.e.,  $d_2 = 1.25 p$ ), is clearly visible in Figure 5b. As the value of the thickness  $d_2$  increased, the values of the reflection



coefficient for  $\lambda = 615$  and  $\lambda = 635$  nm also increased. As a result, it can be stated that for the thicker tested optical system and thicker defect layers, the selective reflection bandwidth was significantly broadened without an undesired decrease in its amplitude.

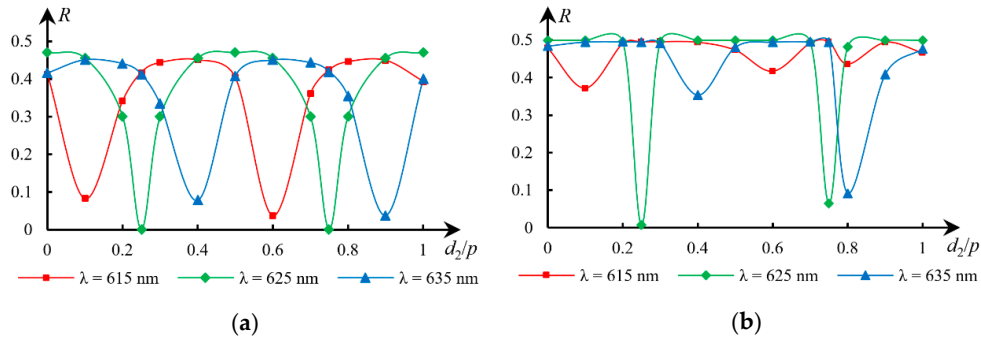


**Figure 6.** Reflection as a function of the thickness  $d_2$  of the defect layer obtained for different values of the wavelength  $\lambda$  of the incident light: (a) *model 1*; (b) *model 2*. The curves interpolated based on the chosen computed values of the reflection represented by markers.

As it has been already noted, the abovementioned numerical tests were obtained for normal incidence of light. However, in our research, we also considered the oblique direction of the incident light. The direction of the beam of obliquely incident light can be described by two angles ( $\theta$  and  $\phi$ ), and it was presented in detail in our previous papers [38,39]. Figure 7 presents color plots of the reflection coefficient  $R$  for the light with the wavelength  $\lambda = 625$  nm incident onto *model 1* and for different values of the thickness  $d_2$ , whereas Figure 8 shows similar plots computed for *model 2*. Numerical simulations presented in Figures 7 and 8 show that the reflection coefficient practically did not change when the angle  $\phi$  changed (especially for thicker layers of the investigated system (see Figure 8), while the distribution of the reflection coefficient changes when the  $\theta$  angle changes. However, for the  $\theta$  angle close to zero (almost perpendicular incidence of light), the reflection coefficient was practically constant. Significant changes could be observed only for large values of the  $\theta$  angle, i.e., around  $80$ – $90^\circ$ .

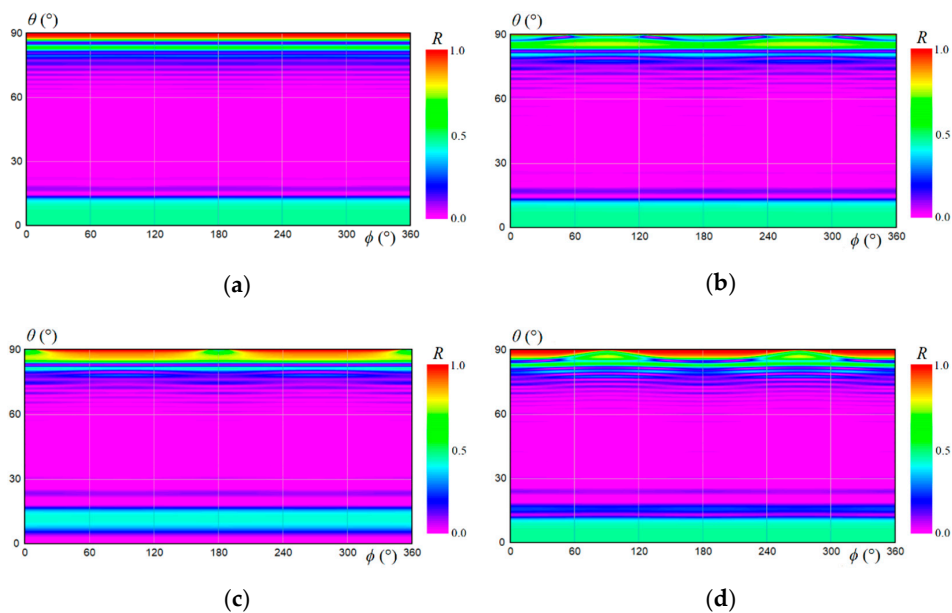


**Figure 7.** Color plots of the reflection coefficient  $R$  (*model 1*) obtained for different values of the thickness  $d_2$  of the defect layer: (a)  $d_2 = 0$ ; (b)  $d_2 = 0.5 p$ ; (c)  $d_2 = 0.75 p$ ; (d)  $d_2 = 3 p$ .

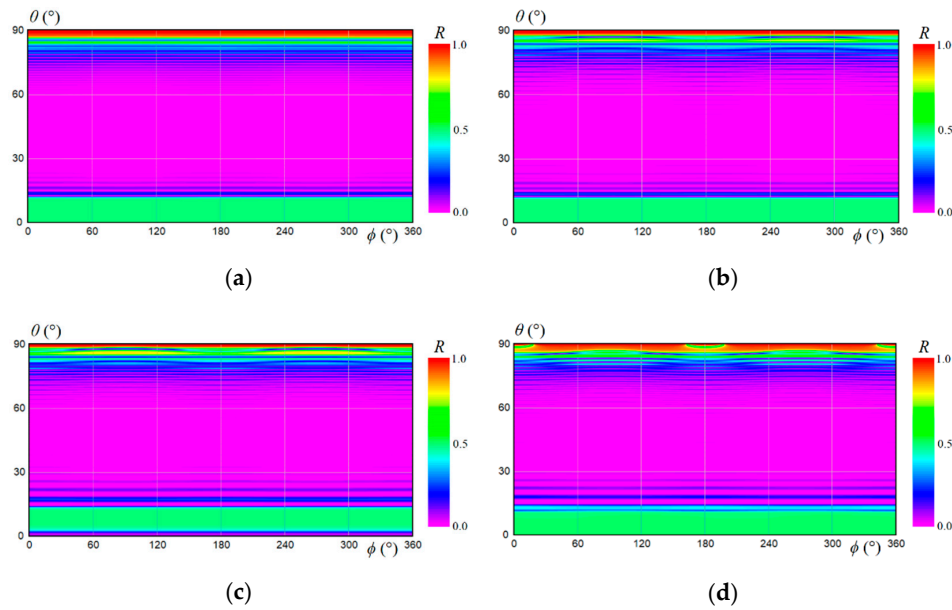
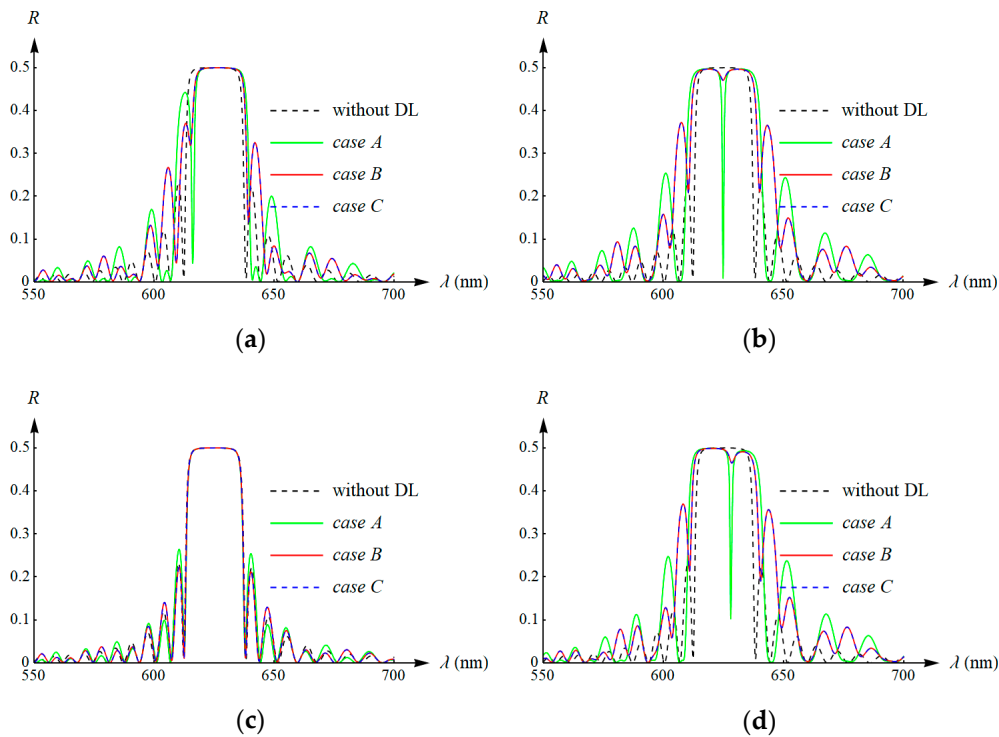


**Figure 8.** Color plots of the reflection coefficient  $R$  (*model 2*) obtained for different values of the thickness  $d_2$  of the defect layer: (a)  $d_2 = 0$ ; (b)  $d_2 = 0.5 p$ ; (c)  $d_2 = 0.75 p$ ; (d)  $d_2 = 3 p$ .

The above figures present the simulations obtained for symmetrical systems ( $d_1 = d_3$ ). Here we also examined the influence of the location of the defect layer inside the investigated CLC cell. To do it, we compared previously tested *model 2* (i.e.,  $d_1 = d_3 = 20 p$ , further referred to as *case A*), with two examples of the asymmetrical location of the defect layer, namely  $d_1 = 10 p$ ,  $d_3 = 30 p$  (further referred to as *case B*) and  $d_1 = 30 p$ ,  $d_3 = 10 p$  (further referred to as *case C*). Again, we considered the case of normal incidence of light first. For comparison, the presented figures also show the case where there was no defect layer (marked as “without DL”). The analysis of the results presented in Figure 9 leads to the conclusion that in asymmetrical systems (i.e., *case B* and *case C*), the spectral curves differed slightly from the curves obtained for the symmetrical system (*case A*). In addition, the influence of the defect location in the reflection spectra for *case B* and *case C* was practically unobservable. Namely, we did not find a significant difference in spectral characteristics between *case B* and *case C*.

We also calculated the reflectance distribution (color plots) for the oblique incident light for all three cases (i.e., *case A*, *case B*, and *case C*). Color plots presenting these calculations in a graphical form are depicted in Figure 10. The presented results (here calculated for  $d_2 = 0.1 p$ ) confirmed the previous conclusions obtained on the basis of spectral curves and distributions of the reflection coefficient. Practically, no differences in the reflection spectra were observed for *case B* and *case C*, which is clearly shown in Figure 10d.

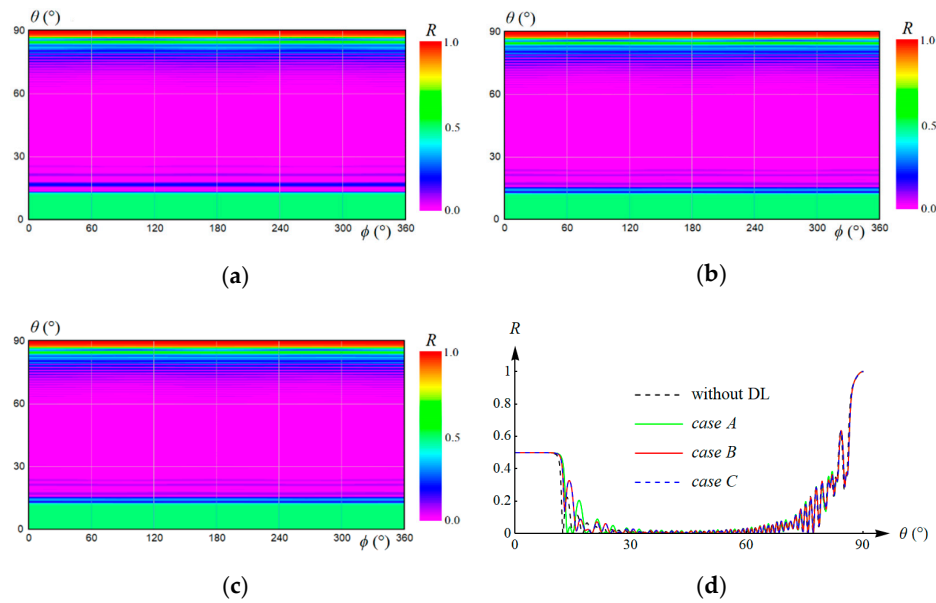
At the end of our research, we analyzed our optical system with a deformed director distribution caused by an externally applied electric field. As it was mentioned in Section 3, from the point of view of the optical properties of the examined system, the spatial distribution of the director field is fundamentally important. Therefore, in the present study, we directly took into account the different director distributions that corresponded to different amplitudes  $E$  of the electric field, without considering material parameters of the examined system. This approach was sufficient for the planned qualitative analysis.



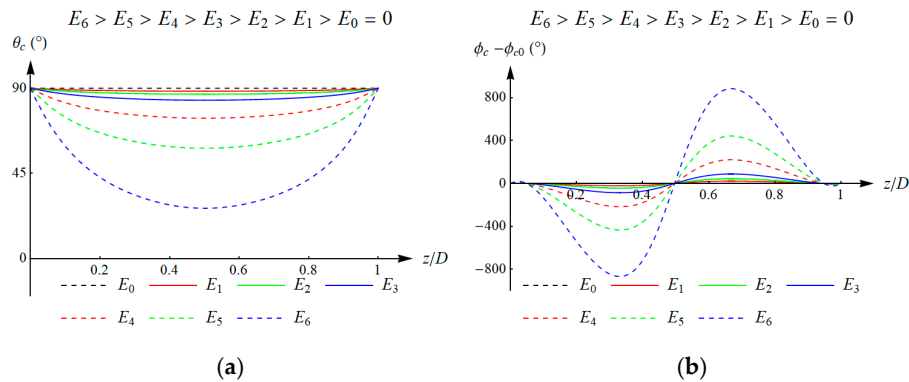
**Figure 9.** Reflection spectra (*model 2*) for different locations of the defect layer and different values of the thickness  $d_2$ : (a)  $d_2 = 0.1 p$ ; (b)  $d_2 = 0.25 p$ ; (c)  $d_2 = 0.5 p$ ; (d)  $d_2 = 0.8 p$ .

Figure 11 presents the applied distributions of the director characterized by the tilt and twist angles as functions of the coordinate  $z$ . For better clarity of the presented results, Figure 11b shows the relative deformations of the angle, i.e.,  $\phi_c - \phi_{c0}$ , in relation to the angle  $\phi_{c0}$  obtained for the case of the undeformed director field. The presented curves correspond to different values of the amplitude  $E$  of the applied electric field, where the following relation was preserved:  $E_6 > E_5 > E_4 > E_3 > E_2 > E_1 > E_0 = 0$ . To increase the transparency of the obtained curves representing the director field, the results were presented together with the curve obtained for the undeformed director field as a reference, i.e., for the electric field  $E_0 = 0$  (plotted by the dashed black curve). As it can be seen, the curves obtained for  $E_1$ ,  $E_2$ , and  $E_3$  were characterized by a relatively low director field deformation, while the curves obtained for  $E_4$ ,  $E_5$ , and  $E_6$  were characterized by a relatively large director field deformation. Therefore, the electric fields with the amplitudes  $E_1$ ,  $E_2$ , and  $E_3$  can be regarded as low electric fields, whereas electric fields with the amplitudes  $E_4$ ,  $E_5$ , and  $E_6$  can be regarded as high electric fields.

For further analysis, we considered only the optical system marked as *model 2*. Figures 12–14 show the spectral reflectance curves obtained for normal incidence of light, when the director field was deformed by an electric field with different amplitudes. The results shown in Figure 12 were obtained for the system without a defect layer ( $d_2 = 0$ ), and the results depicted in Figure 13 were obtained for  $d_2 = 0.25 p$ , whereas Figure 14 presents the results calculated for  $d_2 = 0.5 p$ . Moreover, Figure 12a, Figure 13a, and Figure 14a correspond to the director field deformations obtained for the low electric field ( $E_1$ ,  $E_2$ , and  $E_3$ ), while Figure 12b, Figure 13b, and Figure 14b correspond to the director field deformations obtained for the high electric field ( $E_4$ ,  $E_5$ , and  $E_6$ ). The same results as those depicted in Figures 12–14 are shown again in Figure 15. However, Figure 15 directly shows the influence of different values of the thickness of the defect layer for a fixed director field, i.e., under the given electric field.



**Figure 10.** Color plots of the reflection coefficient (*model 2*) obtained for  $d_2 = 0.1 p$  and different locations of the defect layer: (a) *case A*; (b) *case B*; (c) *case C*. (d) Reflection as a function of the angle  $\theta$  computed for  $\phi = 0$  and different locations of the defect layer.



**Figure 11.** Director field deformations obtained for different values of the amplitudes of the applied electric field: (a) the tilt angle  $\theta_c$ ; (b) the relative deformation of the angle  $\phi_c - \phi_{c0}$  in relation to the angle  $\phi_{c0}$  obtained for the case of the undeformed director field.

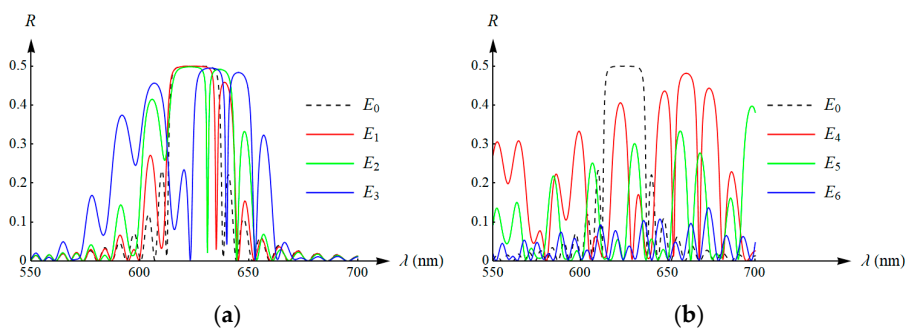


**Figure 12.** Reflection spectra of *model 2* without the defect layer ( $d_2 = 0$ ) calculated for different values of the amplitude of the external applied electric field: (a) low electric field with the amplitudes  $E_1$ ,  $E_2$ , and  $E_3$ ; (b) high electric field with the amplitudes  $E_4$ ,  $E_5$ , and  $E_6$ .

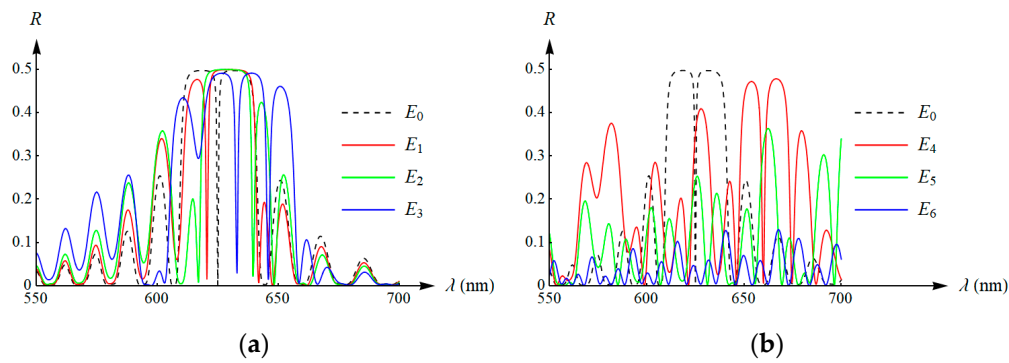


**Figure 13.** Reflection spectra of *model 2* with a defect layer  $d_2 = 0.25 p$  calculated for different values of the amplitude of the external applied electric field: (a) low electric field with the amplitudes  $E_1$ ,  $E_2$ , and  $E_3$ ; (b) high electric field with the amplitudes  $E_4$ ,  $E_5$ , and  $E_6$ .

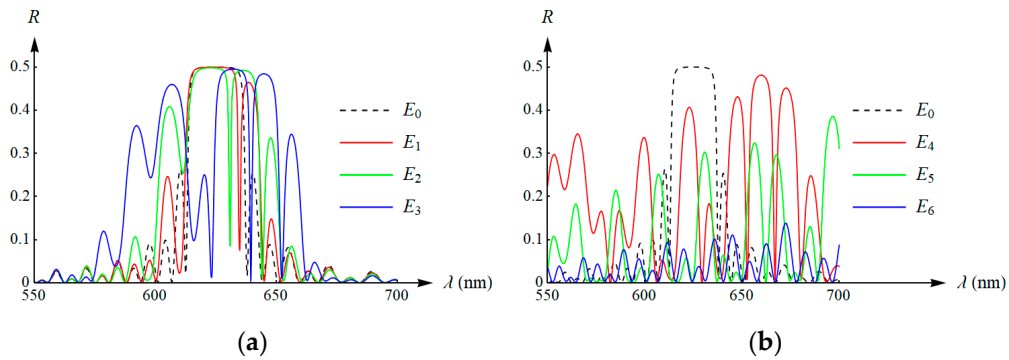


**Figure 14.** Reflection spectra of *model 2* with a defect layer  $d_2 = 0.5 p$  calculated for different values of the amplitude of the external applied electric field: (a) low electric field with the amplitudes  $E_1$ ,  $E_2$ , and  $E_3$ ; (b) high electric field with the amplitudes  $E_4$ ,  $E_5$ , and  $E_6$ .

In the case of the system without a defect layer, the application of a relatively low electric field caused a dip in the spectral curve near the right edge of the bandgap (see Figure 12a). With the increase in the amplitude of the electric field, the existing dip became more visible and shifted toward the short-wave boundary of the bandwidth. As a result, the applied electric field gave a similar effect to the introduction of a defect layer in the case of an undeformed director field of the CLC. What is more, the position of this dip can be precisely tuned within the range of the bandgap that exists for the undeformed director field. Similar conclusions can also be outlined when considering the results presented in Figure 14a that correspond to the system with a defect layer equal to  $0.5 p$ . For the system with the defect layer thickness equal to  $0.25 p$ , a dip in the spectral curve occurred in each presented case (see Figure 13a). For an undeformed director field, this dip was observed in the middle of the bandgap. The application of a low external electric field changed the position of this dip within the bandgap. It is worth noting that the shift of this dip can be both in the direction of the long-wave and the short-wave boundary of the bandwidth, depending on the amplitude of the applied electric field. The observation allowed the change in position of this narrow range. For example, this property can be useful when it is necessary to compensate the position of the dip due to the appearance of undesired external stimuli, such as mechanical or thermal stresses, acting on the considered system. In turn, the analysis of the results presented in Figure 12b, Figure 13b, Figure 14b clearly shows that in a high electric field applied to the tested system with or without a defect layer, the system lost the properties of the selective reflection and the defect modes. Finally, the analysis of the results presented in Figure 15 led to similar conclusions. In particular, for a fixed value of the electric field, the spectral curves were similar for both the system with no defect and the half-wavelength defect layer. In turn,

the spectral curves obtained for the quarter-wavelength defect layer differed significantly from the spectral curves obtained for the system without the defect and with the half-wavelength defect layer, even if the applied electric field had the same value.

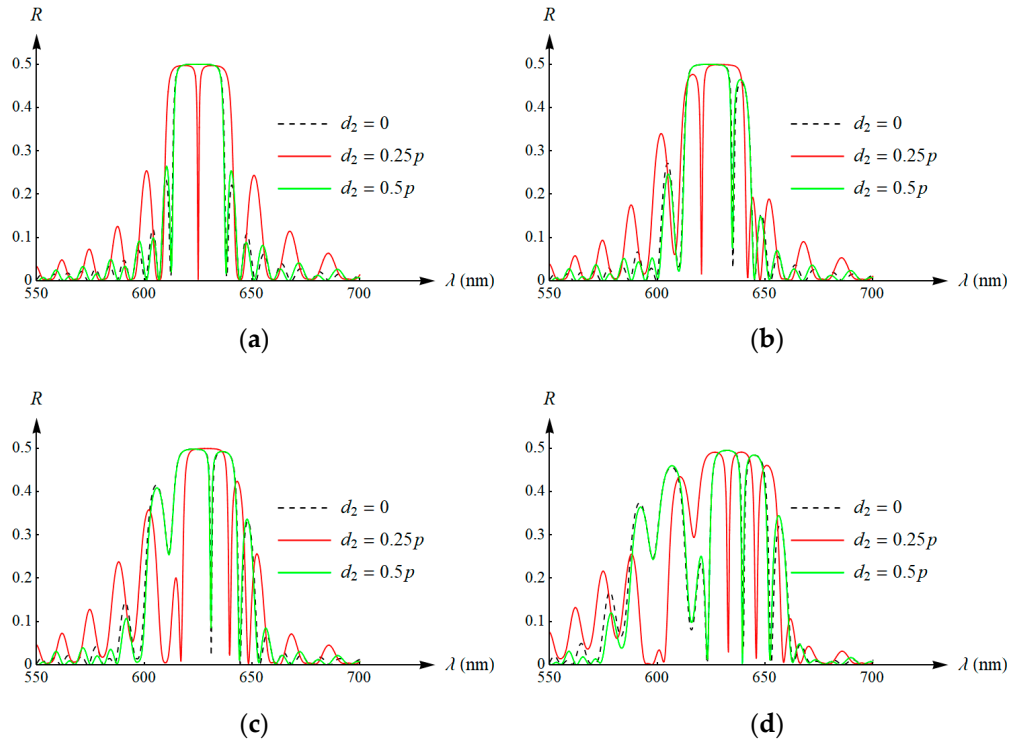


**Figure 15.** Reflection spectra of *model 2* for different thickness of the defect layer and different values of the amplitude of the external applied electric field: (a)  $E = E_0$ ; (b)  $E = E_1$ ; (c)  $E = E_2$ ; (d)  $E = E_3$ .

The results of the present research may be of significant practical importance, since the considered model of the optical system is often found in engineering applications. Namely, in real engineering applications, CLCs are usually sandwiched between two parallel substrates coated with transparent conductive electrode, and voltage is applied across the cell. The applications of such systems can be greatly extended if the reflection can be electrically adjusted. This problem was considered in previous papers. As an example, Yang et al. [46] developed a (polymer network/nematic liquid crystal/chiral dopant) composite exhibiting the bandwidth of the selective reflection spectrum, which is wider and narrower reversibly with increasing and decreasing temperature, respectively. Lu and Chien [47] reported a method of fabricating single-layer color cholesteric liquid crystal displays from a polymer-stabilized cholesteric liquid crystal, where the reflective wavelength can be electrically switched to reflect blue or green from a cell initially reflecting the red color. Bailey et al. [48] investigated the electrical tuning of negative dielectric anisotropy cholesteric liquid crystals under the influence of AC and DC electric fields. They showed an electric effect with potential applications in tunable optical filters, optical pressure/stress sensors, or tunable lasers. In recent years, the application of polymer stabilization in CLCs provides a new dimension to achieve color tuning (for instance, see paper [8] and references cited therein). In the abovementioned paper [8], the authors experimentally investigated the broadening of the reflection band caused by an external electric field applied to the CLC cell. They studied a variety of factors affecting the reflection band broadening of polymer stabilized cholesteric liquid crystals, including the effect of moisture, the effect of alignment layer thickness, the effect of ionic additives, the relation between reflection band broadening and impedance, and the influence of morphology of the polymer network. As a result, by controlling these factors, they observed a wide reflection band to cover the entire visible region under low voltages.



The simulation results presented above concern the analysis of the CLC cell with a defect layer inside and a director field deformed by an external applied electric field. In these studies, we assumed that the spatial director's field distribution could be easily changed by an electric field. In general, studying the dynamic behavior of the considered cholesteric structures in an electric field is not an easy task, and some theoretical aspects in this area can be found in paper [6]. It should also be emphasized that the theoretical stability analysis of the orientation pattern of cholesteric liquid crystals both in electric and magnetic fields has been considered for a few decades. For instance, the unstable behavior of the planar texture between two conducting glass samples at voltages much below those needed to unwind the cholesteric helix was noticed [49]. More intensively, the problem of obtaining a stable and homogeneous uniform lying helix structure has been reported since the late eighties. However, most recently, the developed cholesteric liquid crystal device with the uniform lying helix structure shows stable and reversible characteristics with a short time response [50]. As a result, this enabled the solving of the long-standing problem of stability and hysteresis particularly to meet the manufacturing requirements dedicated to engineering applications.

The presented simulations regarding the appearance of similar defect modes agree with the related theoretical, numerical, or experimental results presented in the literature [51,52], where amplitudes and spectral positions can be elastically tuned. Moreover, our research leads to analogical conclusions as in other references, where it has been demonstrated that the amplitude, the number, and the position of the optical defect modes induced in the bandwidth depend on the thickness, the refractive index, and the anisotropy of the defect layer [17,53–57]. The proposed combination of the study of the defect modes caused by the defect layer inside and the tuning of the optical properties of the system by means of an electric field extends the existing research found in the literature and increases the possibility of its potential real applications.

## 5. Conclusions

First, we investigated the influence of an existing defect in the form of an anisotropic layer sandwiched by CLC. Numerical tests were carried out for different thicknesses of the system, different thicknesses of the defect layer, and different locations of this defect inside the investigated cell. In addition, we also studied the influence of an external electric field applied to the considered optical system that is important from a viewpoint of the technological aspects. Some interesting numerical simulations were obtained, illustrated, and discussed. The results were presented in the form of the reflection spectra for the normal incidence of light or color planar distributions of the reflection coefficient calculated for the oblique incident light. We showed that a defect layer placed inside CLC has a significant influence on the selective reflection phenomenon, and both the shape and the bandwidth of the spectral curve can be tuned by a dopant defect layer. In particular, the results obtained for *model 2* showed that defect modes can have an extremely narrow spectral width (narrow dip in the reflection spectrum or narrow peak in the transmission spectrum) on the order of a few Å.

The considered optical system serves as a model for more complex and realistic cholesteric liquid crystal devices. The obtained numerical results give a new insight into the behavior of practical devices based on the CLC with defect layers and additionally tuned by the external electric field. The analysis presented here demonstrates that there is a significant benefit for the industry to be gained from applying similar methods to models of liquid crystals in more general settings.

The research presented in this paper reflects current issues related to the new approach of modern optics, in which optical properties are determined by geometric factors, including dopants. An example of such a successful implementation is the investigated CLC cell with a defect inside. For instance, such a defect layer with a controlled anisotropy can be created by introducing a layer of a nematic liquid crystal, in which the orientation of the optical axis can be controlled electrically. In other cases, the thickness of the defect layer can be adjusted by the change of the applied voltage. This anisotropic defect provides an additional degree of freedom for tuning the defect modes. As a result, the analyzed CLC with a defect layer can work as an optical diode, which transmits light in one direction and

prevents its propagation in the opposite direction. Currently, such research goals seem justified in engineering due to the expected conversion of electric signals to optical ones.

When it comes to using an external electric field in the considered system, the simplest operating regime is to switch between two states by the sudden application or removal of an electric field. In this way, in the absence of an external electric field, the analyzed system shows a selective reflection, including defect modes resulting from the existing defect layers. By means of small changes in the electric field, it is possible to precisely tune the optical properties of the system, which gives a similar effect to introducing defect layers with different thicknesses. In turn, the application of a high electric field causes the abovementioned optical properties to vanish.

In conclusion, in many technological applications, active tuning and switching of defect modes is desired. By introducing defect layers and applying an external electric field, the propagation of light can be precisely controlled through tailoring of the periodic dielectric structure of the CLC.

**Author Contributions:** Conceptualization, D.G. and J.A.; methodology and software, D.G.; investigation, validation and formal analysis, D.G. and J.A.; writing—original draft preparation and editing, D.G.; supervision and project administration, D.G. and J.A. All authors have read and agreed to the published version of the manuscript.

**Funding:** This research received no external funding.

**Acknowledgments:** We thank to Olga Jarzyna from Department of Automation, Biomechanics and Mechatronics of the Lodz University of Technology for technical support regarding preparation of this manuscript.

**Conflicts of Interest:** The authors declare no conflict of interest.

## References

1. Venkatanarayanan, A.; Spain, E. 13.03—Review of recent developments in sensing materials. In *Comprehensive Materials Processing, Proceedings of the Reference Module in Materials Science and Materials Engineering*; Elsevier: Amsterdam, The Netherlands, 2014; Volume 13, pp. 47–101. [\[CrossRef\]](#)
2. Ramakrishnan, M.; Rajan, G.; Semenova, Y.; Farrell, G. Overview of fiber optic sensor technologies for strain/temperature sensing applications in composite materials. *Sensors* **2016**, *16*, 99. [\[CrossRef\]](#) [\[PubMed\]](#)
3. Beiu, R.-M.; Beiu, V.; Duma, V.-F. Fiber optic mechanical deformation sensors employing perpendicular photonic crystals. *Opt. Express* **2017**, *25*, 23388–23398. [\[CrossRef\]](#) [\[PubMed\]](#)
4. Li, G.; Zhang, S.; Zentgraf, T. Nonlinear photonic metasurfaces. *Nat. Rev. Mater.* **2017**, *2*, 17010. [\[CrossRef\]](#)
5. Beiu, R.-M.; Beiu, V.; Duma, V.-F. Fundamentals and Biomedical Applications of Photonic Crystals: An Overview. In Proceedings of the SPIE 10831, Seventh International Conference on Lasers in Medicine, Timisoara, Romania, 10 August 2018. [\[CrossRef\]](#)
6. Tarasov, O.S.; Krekhov, A.P.; Kramer, L. Dynamics of cholesteric structures in an electric field. *Phys. Rev. E* **2003**, *68*, 031708. [\[CrossRef\]](#)
7. Kopp, V.I.; Genack, A.Z. Twist defect in chiral photonic structures. *Phys. Rev. Lett.* **2002**, *89*. [\[CrossRef\]](#)
8. Nemati, H.; Liu, S.; Moheghi, A.; Tondiglia, V.P.; Lee, K.M.; Bunning, T.J.; Yang, D.-K. Enhanced reflection band broadening in polymer stabilized cholesteric liquid crystals with negative dielectric anisotropy. *J. Mol. Liq.* **2018**, *267*, 120–126. [\[CrossRef\]](#)
9. Kopp, V.I.; Bose, R.; Genack, A.Z. Transmission through chiral twist defects in anisotropic periodic structures. *Opt. Lett.* **2003**, *28*, 349–351. [\[CrossRef\]](#)
10. Yang, Y.-C.; Kee, C.-S.; Kim, J.-E.; Park, H.Y. Photonic defect modes of cholesteric liquid crystals. *Phys. Rev. E* **1999**, *60*, 6852–6854. [\[CrossRef\]](#)
11. Yablonovitch, E.; Gmitter, T.J.; Meade, R.D.; Rappe, A.M.; Brommer, K.D.; Joannopoulos, J.D. Donor and acceptor modes in photonic band structure. *Phys. Rev. Lett.* **1991**, *67*, 3380–3383. [\[CrossRef\]](#)
12. Hodgkinson, I.J.; Wu, Q.H.; Thorn, K.E.; Lakhtakia, A.; McCall, M.W. Spacerless circular-polarization spectral-hole filters using chiral sculptured thin films: Theory and experiment. *Opt. Commun.* **2000**, *184*, 57–66. [\[CrossRef\]](#)
13. Schmidtke, J.; Stille, W.; Finkelmann, H. Defect mode emission of a dye doped cholesteric polymer network. *Phys. Rev. Lett.* **2003**, *90*, 083902. [\[CrossRef\]](#)
14. Yokoyama, H.; Suzuki, M.; Nambu, Y. Spontaneous emission and laser oscillation properties of microcavities containing a dye solution. *Appl. Phys. Lett.* **1991**, *58*, 2598–2600. [\[CrossRef\]](#)

15. Painter, O.; Lee, R.K.; Scherer, A.; Yariv, A.; O'Brien, J.D.; Dapkus, P.D.; Kim, I. Two-dimensional photonic band-gap defect mode laser. *Science* **1999**, *284*, 1819–1821. [\[CrossRef\]](#)
16. Belyakov, V. *Diffraction Optics of Complex—Structured Periodic Media. Localized Optical Modes of Spiral Media*, 2nd ed.; Springer Nature Switzerland AG ©: Cham, Switzerland, 2019.
17. Gevorgyan, A.H.; Harutyunyan, M.Z. Chiral photonic crystals with an anisotropic defect layer. *Phys. Rev. E* **2007**, *76*, 031701-1–031701-9. [\[CrossRef\]](#)
18. Gevorgyan, A.A.; Papoyan, K.V.; Pikichyan, O.V. Reflection and transmission of light by cholesteric liquid crystal-glass-cholesteric liquid crystal and cholesteric liquid crystal(1)-cholesteric crystal(2) systems. *Opt. Spectrosc.* **2000**, *88*, 586–593. [\[CrossRef\]](#)
19. Gu, C.; Yeh, P. Extended Jones matrix method and its application in the analysis of compensators for liquid crystal displays. *Displays* **1999**, *20*, 237–257. [\[CrossRef\]](#)
20. Ozaki, M.; Ozaki, R.; Matsui, T.; Yoshino, K. Twist-defect-mode lasing in photopolymerized cholesteric liquid crystal. *Jpn. J. Appl. Phys.* **2003**, *42*, 472–475. [\[CrossRef\]](#)
21. Ha, N.Y.; Takanishi, Y.; Ishikawa, K.; Takezoe, H. Simultaneous RGB reflections from single-pitched cholesteric liquid crystal films with Fibonacci defects. *Opt. Express* **2007**, *15*, 1024–1029. [\[CrossRef\]](#)
22. Matsui, T.; Ozaki, M.; Yoshino, K. Tunable photonic defect modes in a cholesteric liquid crystal induced by optical deformation of helix. *Phys. Rev. E* **2004**, *69*, 061715. [\[CrossRef\]](#)
23. Chen, J.-Y.; Chen, L.W. Defect modes in a stacked structure of chiral photonic crystals. *Phys. Rev. E* **2005**, *71*, 061708. [\[CrossRef\]](#)
24. Song, M.H.; Ha, N.; Amemiya, K.; Park, B.; Takanishi, Y.; Ishikawa, K.; Wu, J.; Nishimura, S.; Takezo, H. Defect-mode lasing with lowered threshold in a three-layered hetero-cholesteric liquid-crystal structure. *Adv. Mater.* **2006**, *18*, 193–197. [\[CrossRef\]](#)
25. Ozaki, R.; Matsuhisa, Y.; Yoshida, H.; Yoshino, K.; Ozaki, M. Optical properties and electric field enhancement in cholesteric liquid crystal containing different periodicities. *J. Appl. Phys.* **2006**, *100*, 023102. [\[CrossRef\]](#)
26. Ha, N.Y.; Jeong, S.M.; Nishimura, S.; Suzuki, G.; Ishikawa, K.; Takezoe, H. Simultaneous red, green, and blue lasing emissions in a single-pitched cholesteric liquid-crystal system. *Adv. Mater.* **2008**, *20*, 2503–2507. [\[CrossRef\]](#)
27. Nascimento, E.M.; Zanetti, F.M.; Lyra, M.L.; de Oliveira, I.N. Tunable reflectance spectra of multilayered cholesteric photonic structures with anisotropic defect layers. *Phys. Rev. E* **2010**, *81*, 031713. [\[CrossRef\]](#)
28. He, Z.; Ye, Z.; Cui, Q.; Zhu, J.; Gao, H.; Ling, Y.; Cui, H.; Lu, J.; Guo, X.; Su, Y. Reflection chromaticity of cholesteric liquid crystals with sandwiched periodical isotropic defect layers. *Opt. Commun.* **2011**, *284*, 4022–4027. [\[CrossRef\]](#)
29. Gevorgyan, A.H. Tunable reflectance of a two-defect-layer cholesteric liquid crystal. *Phys. Rev. E* **2011**, *83*, 011702. [\[CrossRef\]](#)
30. Vetrov, S.Y.; Pyatnov, M.V.; Timofeev, I.V. Photonic defect modes in a cholesteric liquid crystal with a resonant nanocomposite layer and a twist defect. *Phys. Rev. E* **2014**, *90*, 032505. [\[CrossRef\]](#)
31. Yang, O.; Wang, Y.; Wang, H.; Yanling, H.; Peng, J. Effect of stress-induced anisotropy on localized mode of one-dimensional photonic crystal with mirror symmetry. *Optik* **2015**, *126*, 5583–5586. [\[CrossRef\]](#)
32. Yang, D.-K.; Wu, S.-T. *Fundamentals of Liquid Crystal Devices*, 2nd ed.; John Wiley & Sons, Ltd.: Hoboken, NJ, USA, 2014. [\[CrossRef\]](#)
33. Ericksen, J.L. Equilibrium theory of liquid crystals. *Adv. Liq. Cryst.* **1976**, *2*, 233–298. [\[CrossRef\]](#)
34. Leslie, F.M. *Theory of Flow Phenomena in Nematic Liquid Crystals*; Ericksen, J.L., Kinderlehrer, D., Eds.; Springer: New York, NY, USA, 1987. [\[CrossRef\]](#)
35. Leslie, F.M. Continuum theory for nematic liquid crystals. *Contin. Mech. Thermodyn.* **1992**, *4*, 167–175. [\[CrossRef\]](#)
36. Self, R.H.; Please, C.P.; Sluckin, T.J. Deformation of nematic liquid crystals in an electric field. *Eur. J. Appl. Math.* **2002**, *13*, 1–23. [\[CrossRef\]](#)
37. Gevorgyan, A.H. About defect mode peculiarities in cholesteric liquid crystals with anisotropic defect layer inside. *Optik* **2018**, *154*, 656–661. [\[CrossRef\]](#)
38. Grzelczyk, D.; Awrejcewicz, J. Reflectance and transmittance of cholesteric liquid crystal sandwiched between polarizers. In *Springer Proceedings in Mathematics & Statistics*; Awrejcewicz, J., Ed.; Springer: Cham, Switzerland, 2018; Volume 249, pp. 147–158. [\[CrossRef\]](#)

39. Grzelczyk, D.; Awrejcewicz, J. Calculation of reflectance and transmittance of optical birefringent networks based on cholesteric liquid crystals. *Latin Am. J. Solids Struct.* **2019**, *16*, 20. [\[CrossRef\]](#)
40. Yeh, P.; Gu, C. *Optics of Liquid Crystal Displays*; John Wiley and Sons: New York, NY, USA, 1999.
41. Chen, C.-J.; Lien, A.; Nathan, M.I.  $4 \times 4$  matrix method for biaxial media and its application to liquid crystal displays. *Jpn. J. Appl. Phys.* **1996**, *35*, 1204–1207. [\[CrossRef\]](#)
42. Ivanov, O.V.; Sementsov, D.I. Light propagation in stratified chiral media. The  $4 \times 4$  matrix method. *Crystallogr. Rep.* **2000**, *45*, 487–492. [\[CrossRef\]](#)
43. Abdulhalim, I. Analytic propagation matrix method for anisotropic magneto-optic layered media. *J. Opt. A Pure Appl. Opt.* **2000**, *2*, 557–564. [\[CrossRef\]](#)
44. Lakhtakia, A.; Reyes, A. Theory of electrically controlled exhibition of circular Bragg phenomenon by an obliquely excited structurally chiral material—Part 1: Axial dc electric field. *Optik* **2008**, *119*, 253–268. [\[CrossRef\]](#)
45. Ortega, J.; Folcia, C.L.; Etxebarria, J. Upgrading the performance of cholesteric liquid crystal lasers: Improvement margins and limitations. *Materials* **2018**, *11*, 5. [\[CrossRef\]](#)
46. Yang, H.; Mishima, K.; Matsuyama, K.; Hayashi, K.-I.; Kikuchi, H.; Kajiyama, T. Thermally bandwidth-controllable reflective polarizers from (polymer network/liquid crystal/chiral dopant) composites. *Appl. Phys. Lett.* **2003**, *82*, 2407–2409. [\[CrossRef\]](#)
47. Lu, S.-Y.; Chien, L.-C. A polymer-stabilized single-layer color cholesteric liquid crystal display with anisotropic reflection. *Appl. Phys. Lett.* **2007**, *91*, 131119. [\[CrossRef\]](#)
48. Bailey, C.A.; Tondiglia, V.P.; Natarajan, L.V.; Duning, M.M.; Bricker, R.L.; Sutherland, R.L.; White, T.J.; Durstock, M.F.; Bunning, T.J. Electromechanical tuning of cholesteric liquid crystals. *J. Appl. Phys.* **2010**, *107*, 013105. [\[CrossRef\]](#)
49. Helfrich, W. Deformation of cholesteric liquid crystals with low threshold voltage. *Appl. Phys. Lett.* **1970**, *17*, 531–532. [\[CrossRef\]](#)
50. Yip, W.C.; Welch, C.; Mehl, G.H.; Wilkinson, T.D. A cholesteric liquid crystal device having stable uniform lying helix structure. *J. Mol. Liq.* **2020**, *299*, 112141. [\[CrossRef\]](#)
51. Avendanno, C.G.; Martinez, D. Elastic dependence of defect modes in one-dimensional photonic crystals with a cholesteric elastomer slab. *Photonics Nanostruct. Fundam. Appl.* **2018**, *30*, 30–38. [\[CrossRef\]](#)
52. Matsuhisa, Y.; Ozaki, R. High Q defect mode and laser action in one-dimensional hybrid photonic crystal containing cholesteric liquid crystal. *Appl. Phys. Lett.* **2006**, *89*, 101109. [\[CrossRef\]](#)
53. Ozaki, R.; Matsui, T.; Ozaki, M.; Yoshino, K. Electro-tunable defect mode in one-dimensional periodic structure containing nematic liquid crystal as a defect layer. *Jpn. J. Appl. Phys.* **2002**, *41*, 1482–1484. [\[CrossRef\]](#)
54. Ozaki, R.; Ozaki, M.; Yoshino, K. Defect mode switching in one-dimensional photonic crystal with nematic liquid crystal as defect layer. *Jpn. J. Appl. Phys.* **2003**, *42*, 669–671. [\[CrossRef\]](#)
55. Ozaki, R.; Ozaki, M.; Yoshino, K. Defect mode in one-dimensional photonic crystal with in-plane switchable nematic liquid crystal defect layer. *Jpn. J. Appl. Phys.* **2004**, *43*, 1477–1479. [\[CrossRef\]](#)
56. Arkhipkin, V.G.; Gunyakov, V.A.; Myslivets, S.A.; Gerasimov, V.P.; Zyryanov, V.Y.; Vetrov, S.Y.; Shabanov, V.F. One-dimensional photonic crystals with a planar oriented nematic layer: Temperature and angular dependence of the spectra of defect modes. *J. Exp. Theor. Phys.* **2008**, *106*, 388–398. [\[CrossRef\]](#)
57. Kumar, R.; Kumar, D.; Kushwaha, A.S.; Srivastava, S.K. Study of one-dimensional nanolayered graded photonic crystal consisting of birefringent and dielectric materials. *Photonics Nanostruct. Fundam. Appl.* **2018**, *28*, 20–31. [\[CrossRef\]](#)

